Research Article

Journal of RAMAN SPECTROSCOPY

Received: 16 March 2010 Accepted: 14 May 2010 Published online in Wiley Online Library: 28 June 2010

(wileyonlinelibrary.com) DOI 10.1002/jrs.2725

Raman polarization analysis of highly crystalline polyethylene fiber

Leonardo Puppulin, Yasuhito Takahashi, Wenliang Zhu and Giuseppe Pezzotti*

The complex orientation dependence in space of Raman active vibrations in the orthorhombic structure of polyethylene (PE) is discussed in terms of Raman tensor elements as intrinsic physical parameters of the lattice. Building upon the symmetry assignment of these vibrational modes, we systematically studied, from both theoretical and experimental viewpoints, the changes of polarized intensity for the A_g and the $B_{2g} + B_{3g}$ vibrational modes with respect to PE molecular orientation. After explicitly expanding the Raman selection rules associated with the A_g and the $B_{2g} + B_{3g}$ modes, introducing them into general expressions of the orientation distribution function, and validating them by means of a least-square fitting procedure on experimental data, we compare here two mesostructural models for a highly crystallized and self-aligned PE fiber structure. Stereological arguments are shown concerning the arrangement of orthorhombic fibrils in such a sample that unfold the correct values of five independent Raman tensor elements for orthorhombic PE.

Supporting information may be found in the online version of this article.

Keywords: Raman tensor; polyethylene; polarized Raman spectroscopy; molecular orientation; orthorhombic structure

Introduction

Polyethylene (PE) has been thoroughly studied in the past 60 years, being the largest volume polymer consumed in the world. Renewed interest in the structural characteristics of PE arises from the fact that this material is used as a bearing material in orthopedic joint components (e.g. knee and hip prostheses). This is due to its low friction coefficient, its high wear resistance and biocompatibility, which are among the highest for polymers.[1–3] The continuously rising demand of long-term durability of such implants in low-friction arthroplasty has stimulated the efforts of scientists and technologists in developing PE structures less prone to generation of micrometric wear debris. As a matter of fact, the byproducts of wear degradation are the most detrimental cause of failure for PE-bearing components embedded in the human body, since body reaction to such foreign particles leads to irreversible bone degeneration.[4–6] The need for better understanding the basics of PE structures and to expand their methods of analysis, indeed, represented the main driving force of this study.

We and other research groups have been recently involved with studies concerning the improvement of both the oxidation and wear behavior of PE bearings exposed in the human body. In this context, since crystallographic information is very relevant to successful molecular design of the surface of advanced biomedical components,[7–10] the development of a fully three-dimensional analysis of the molecular orientation of the PE orthorhombic structure is mandatory. Raman microprobe spectroscopy offers a viable path to assess the (local) orientation in PE components. It was demonstrated that the best window to characterize medium- to long-range organization of macromolecules in high- and semi-crystalline fibers is the low wavenumber region where the collective/lattice modes are located.[11] However, the analysis of Raman band characteristics in the middle wavenumber range of crystalline macromolecules has also been widely used as an alternative procedure,[12] although bands in such a spectral region only probe local structures. Moreover, in order to make the method quantitative and to detect stereological changes of molecular orientation due to mechanical action, it is necessary to fully resolve the second-rank tensor associated with the vibrational bands of a partially aligned orthorhombic PE structure. In this paper, we first present a theoretical description of the periodic dependences under polarized light of the A_g and $B_{2g} + B_{3g}$ phonon mode intensities on the set of three Euler angles between the laser polarization direction and the crystallographic axes of the orthorhombic structure of PE. Then, we validate the obtained Raman selection rules with experimental data collected by performing a set of polarized Raman experiments on a highly crystalline PE fiber from which we calculate a set of five independent Raman tensor components.

Experimental

The investigated sample was a monofilament of a commercially available ultrahigh molecular weight PE fiber manufactured by Ningbo Dancheng Advanced Materials Co. Ltd (Zhejiang, China). Raman spectra were collected at room temperature by a triple monochromator (T-64000, Jobin-Yvon/Horiba Group, Kyoto, Japan) equipped with a charge-coupled device detector,

* *Correspondence to: Giuseppe Pezzotti, Ceramic Physics Laboratory & Research Institute for Nanoscience (RIN), Kyoto Institute of Technology, Sakyo-ku, Matsugasaki, 606-8585 Kyoto, Japan. E-mail: pezzotti@kit.ac.jp*

Ceramic Physics Laboratory & Research Institute for Nanoscience (RIN), Kyoto Institute of Technology, Matsugasaki, 606-8585 Kyoto, Japan

Journal of RAMAN SPECTROSCOPY

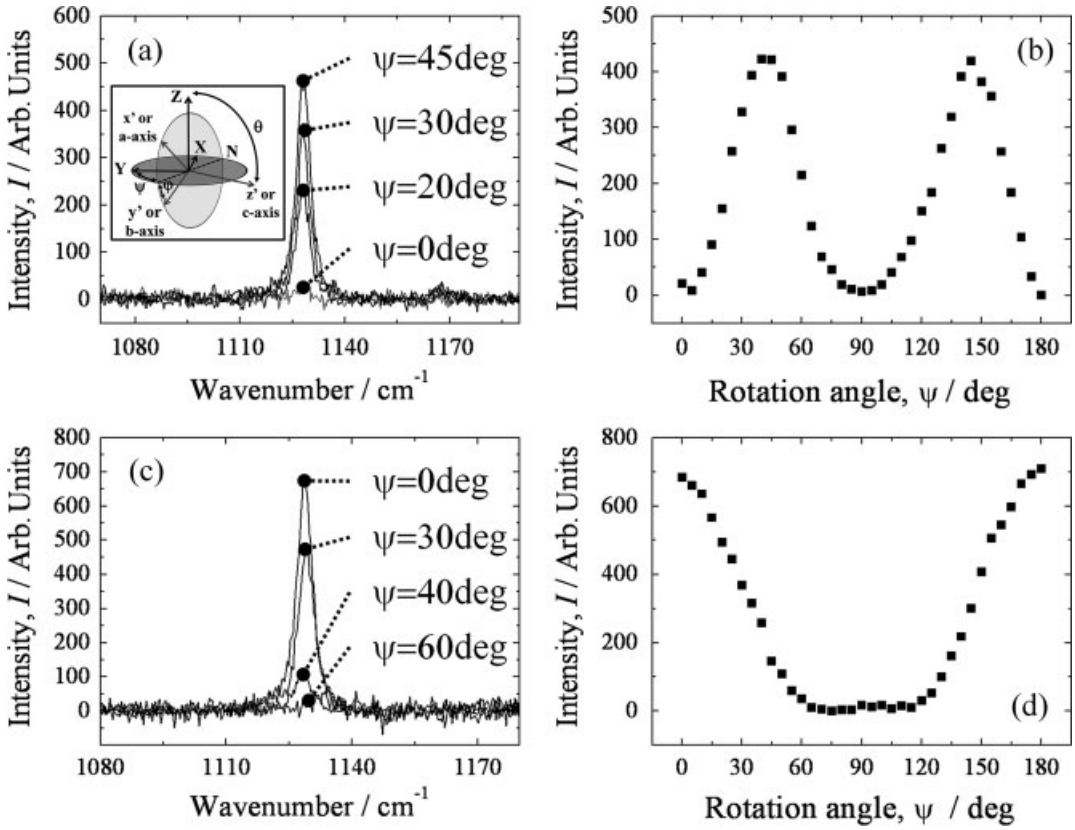

Figure 1. A_g Raman bands as collected in cross (a) and parallel (c) probe polarization geometries, as a function of rotation angle ψ on a PE fiber. In (b) and (d), we report typical experimental plots of the angular dependence of Raman scattering intensities (A_g mode) collected by rotating in-plane the fiber axis (for cross and parallel polarization, respectively). A schematic draft of the adopted Cartesian reference system is shown in inset of (a), with the Euler angles that correlate the laboratory reference system (*XYZ*) to the crystallographic reference system ($x'y'z'$) of the PE fiber.

and analyzed by using commercially available software (Labspec, Horiba/Jobin-Yvon Group). The excitation source was the monochromatic blue line emitted by an Ar ion laser at 488 nm (Stabilite 2017; Spectra Physics, Mountain View, CA) with a power of 100 mW. The crystallinity of the fiber sample was as high as 99.8%, as determined from its nonpolarized Raman spectrum according to the method given by Strobl and Hagedorn.[13] In inset of Fig. 1(a), a schematic sketch is shown that explains our choice of laboratory reference system with respect to the crystal reference system in terms of Euler angles in space.

Results and Discussion

A literature review of the studies in the past four decades,[14–16] which were based on small- and wide-angle X-ray measurements, shows evidence that PE fibers generally possess a high degree of uniaxial orientation and remarkably higher degrees of crystallinity as compared to bulk PE samples. The crystalline phase in the fiber is predominantly orthorhombic and, due to the strongly unidirectional deformation that takes place during the drawing process, PE molecular chains are highly aligned along the long axis of the fiber.[17] In other words, the typical spherulitic structure characteristic of undeformed PE is converted during drawing into a fibrillar structure in which the *c* axis of the orthorhombic cell is parallel to the drawing direction. However, the lack of spatial resolution in the characterization techniques available so far (i.e. including Raman microprobe spectroscopy) does not allow to univocally locate the orientation of the *a* and *b* axis in the *c* plane of the orthorhombic cell. This circumstance, together with the difficulty in obtaining an orthorhombic PE single crystal with homogeneous orientation, is the reason for the partially unknown structure of the Raman tensor of PE. In this study, we attempt to correct this lack of understanding and to pass over the spatial resolution issues by tackling the problem from a stereological viewpoint. For doing so, we matched highly spectrally resolved (polarized) Raman data with two different, but in principle both realistic, structural models describing the arrangement in space of the PE orthorhombic fibrils on the mesoscale.

Rieckel *et al*.[18] studied a highly oriented PE fiber by collecting diffraction patterns by means of a 2-μm X-ray beam. Their results of scanning along the diameter of the fiber suggested the presence of blocks of orthorhombic domains with size typically in the order of the tens of micrometers, which only differed in the preferred orientation of their *b* axis. According to this model (henceforth simply referred to as Model I), we can assume that our confocal/polarized Raman probe (whose size has been quantitatively calibrated in a previous study[19] as 2.2 and 6.4 μm in diameter and depth, respectively) might eventually span an individual homogeneously oriented orthorhombic domain. On the other hand, Dees and Spruiell[20] put forward a stereological model for drawn PE fibers that foresees PE lamellae consisting of sub-micrometric fibril nuclei radially grown outward, the

growth direction being along the *b* axis of orthorhombic PE. According to this latter model (henceforth simply referred to as Model II), the crystalline structure of a PE fiber can be considered to be isotropic in any plane perpendicular to the fiber axis. In other words, if this structural model were valid, our confocal/polarized Raman probe would not be capable of resolving any preferential orientation in a plane perpendicular to the long fiber axis. Figure S1 (Supporting Information) shows sketches of the interaction between the confocal/polarized Raman probe and the PE fiber in the cases of both the aforementioned structural models. The tensorial rules governing the relative intensity of the Raman bands for a given crystal structure can be expressed as a function of crystal orientation in space and probe polarization geometry,[21–22] according to the following tensorial equation:

$$I \propto |\mathbf{e}_i \Re \mathbf{e}_s|^2 \tag{1}$$

where I is the scattered Raman intensity, $\mathbf{e}_i$ and $\mathbf{e}_s$ are the unit polarization vectors of the electric field for incident and scattered light, respectively. For a fixed polarization vector of the incident light (which is the case with our Raman equipment), parallel and cross-polarization geometries are thus possible for the scattered light, the unit polarization vectors being expressed in Cartesian coordinates, as follows:

$$\mathbf{e}^{||}_{ixyz} = (0 \quad 1 \quad 0), \quad \mathbf{e}^{||}_{sxyz} = \begin{pmatrix} 0 \\ 1 \\ 0 \end{pmatrix}, \quad \mathbf{e}^{\perp}_{sxyz} = \begin{pmatrix} 1 \\ 0 \\ 0 \end{pmatrix} \tag{2}$$

where the subscripts *i* and *s* refer to the incident and scattered light, respectively; the superscripts || and ⊥ refer to the parallel and cross configuration of the polarized probe, respectively $(Z(YY)\overline{Z}$ and $Z(YX)\overline{Z}$, respectively, in Porto notations[23]). $\Re$ is referred to as the second-rank Raman scattering tensor of the particular vibrational mode under consideration (Table 1), whose set of five independent elements are the object of this study. In this analysis, we considered the bands of PE Raman spectrum located at 1130 and 1293 cm^{-1}; these bands are related to the C–C stretching vibration (A_g mode) and the -CH_2- twisting vibration ($B_{2g} + B_{3g}$ mode), respectively. The tensorial Eqn (1) can be explicitly expressed in terms of three Euler angles in space by using a transformation matrix and its inverse. Then, the general angular dependences (also referred to as the Raman selection rules) can be derived for both cases of structural models reported for the structure of the PE fiber (Fig. S1). Table 1 lists the structure of the Raman tensors for the A_g and $B_{2g} + B_{3g}$ modes,[24] expressed in the crystal principal axis directions, and the Raman selection rules pertaining to the two structural models describing the microstructure of the crystalline fiber. In such equations, Λ and γ represent numerical constants that depend on the instrumental configuration and spectral band employed. As far as Model I is concerned, in our reference choice (inset in Fig. 1(a)), $\boldsymbol{\theta}$ is expected to be very close to $\boldsymbol{\pi}/2$ (given the expected high degree of alignment of the fiber), $\boldsymbol{\psi}$ corresponds to the in-plane rotation angle of the jig supporting the fiber (the variable angle in our experiments), while $\boldsymbol{\varphi}$ is the angle describing the orientation of the *b* and *a* axis in the *c* plane, which is unknown. Moreover, the selection rules reported in Table 1 invariably show that the periodicity of the Raman intensity fluctuation could be expected over either an interval $0 \leq \boldsymbol{\psi} \leq \boldsymbol{\pi}$ or $0 \leq \psi \leq \pi/2$, depending on the examined Raman mode. Figure 1 experimentally proves the actual existence of different periodicities as theoretically predicted for Raman intensities under different polarization geometries. However, in order to obtain a fully quantitative Raman assessment, the local orientation distribution function of the molecular chains has to be taken into consideration in the computations.[25–27] Such functions have been formulated in terms of Wigner functions expanded in series of Legendre polynomials. A set of four working equations that include both Raman selection rules and molecular distribution patterns can be given[28]:

$$I^{||,\perp}_{A_g}(\theta,\varphi,\psi) = \frac{\int_{\gamma=0}^{\gamma=2\pi}\int_{\alpha=0}^{\alpha=2\pi}\int_{\beta=0}^{\beta=\pi} I^{||,\perp}_{A_g}(\beta',\varphi,\psi) f(\beta)\sin\beta\, d\beta\, d\alpha\, d\gamma}{\int_{\gamma=0}^{\gamma=2\pi}\int_{\alpha=0}^{\alpha=2\pi}\int_{\beta=0}^{\beta=\pi} f(\beta)\sin\beta\, d\beta\, d\alpha\, d\gamma} \tag{3}$$

$$I^{||,\perp}_{B_{2g}+B_{3g}}(\theta,\varphi,\psi) = \frac{\int_{\gamma=0}^{\gamma=2\pi}\int_{\alpha=0}^{\alpha=2\pi}\int_{\beta=0}^{\beta=\pi} I^{||,\perp}_{B_{2g}+B_{3g}}(\beta',\varphi,\psi) f(\beta)\sin\beta\, d\beta\, d\alpha\, d\gamma}{\int_{\gamma=0}^{\gamma=2\pi}\int_{\alpha=0}^{\alpha=2\pi}\int_{\beta=0}^{\beta=\pi} f(\beta)\sin\beta\, d\beta\, d\alpha\, d\gamma} \tag{4}$$

with the Raman intensities in the integrals given in Table 1; (α,β,γ) represent an additional set of Euler angles that describes the molecular orientation within the probe and are linked to the set of Euler angles (θ,φ,ψ), describing the orientation of the fiber in space, according to the following equation:

$$\beta' = \frac{\pi}{2} - \theta = \arctan\left(\frac{\tan\beta}{\sqrt{\tan^2\alpha + 1}}\right) \tag{5}$$

The orientation distribution function $f(\beta)$ is given as:

$$f(\beta) = A\exp\{-[\lambda_2 P_2(\cos\beta) + \lambda_4 P_4(\cos\beta)]\} \tag{6}$$

where A is a constant and the parameters λ_2 and λ_4 are the Lagrange multipliers used in the definition of the principle of maximum information entropy reported by Jaynes.[29] The three parameters A, λ_2 and λ_4 can be determined by solving the system of three equations, which describe the average values of the Legendre polynomials:

$$\int_{\gamma=0}^{\gamma=2\pi}\int_{\alpha=0}^{\alpha=2\pi}\int_{\beta=0}^{\beta=\pi} f(\alpha,\beta,\gamma)\sin\beta\, d\beta\, d\alpha\, d\gamma = 1 \tag{7}$$

$$\int_{\gamma=0}^{\gamma=2\pi}\int_{\alpha=0}^{\alpha=2\pi}\int_{\beta=0}^{\beta=\pi} P_2(\cos\beta) f(\beta)\sin\beta\, d\beta\, d\alpha\, d\gamma = \langle P_2(\cos\beta)\rangle \tag{8}$$

$$\int_{\gamma=0}^{\gamma=2\pi}\int_{\alpha=0}^{\alpha=2\pi}\int_{\beta=0}^{\beta=\pi} P_4(\cos\beta) f(\beta)\sin\beta d\beta d\alpha d\gamma = \langle P_4(\cos\beta)\rangle \tag{9}$$

Of the two 'order parameters' $\langle P_2(\cos\beta)\rangle$ and $\langle P_4(\cos\beta)\rangle$, the former is usually referred to as the Herman's orientation parameter.[28] This parameter assumes the value zero when the orientation of the orthorhombic crystals is fully random, while the values 1 and −0.5 are assumed when perfect orientation along and perpendicular to a given axis (e.g. the long axis of the fiber) is reached, respectively. The Herman's orientation parameter is the primary parameter to judge the alignment of crystalline

Table 1. Raman tensor elements and the predicted dependences of polarized Raman intensities on crystallographic orientation for the A_g and the $B_{2g} + B_{3g}$ modes, according to Raman selection rules[a]

Model I		$\Re_{Ag} = \begin{vmatrix} a & 0 & 0 \\ 0 & b & 0 \\ 0 & 0 & c \end{vmatrix}$ $\Re_{B_{2g}+B_{3g}} = \begin{vmatrix} 0 & 0 & e \\ 0 & 0 & f \\ e & f & 0 \end{vmatrix}$
A_g	Cross	$I = \Lambda \begin{bmatrix} 0.5(b-a)\cos\theta \sin 2\varphi \cos 2\psi + \sin\psi \cos\psi (a\sin^2\varphi + b\cos^2\varphi - c\sin^2\theta) \\ -\cos^2\theta \sin\psi \cos\psi (a\cos^2\varphi + b\sin^2\varphi) \end{bmatrix}^2 + \gamma$
	Parallel	$I = \Lambda \begin{bmatrix} c\sin^2\theta \sin^2\psi + a(\sin\varphi\cos\psi + \cos\theta\cos\varphi\sin\psi)^2 \\ +b(\cos\varphi\cos\psi - \cos\theta\sin\varphi\sin\psi)^2 \end{bmatrix} + \gamma$
$B_{2g} + B_{3g}$	Cross	$I = \Lambda \begin{Bmatrix} 0.5\times[-e\sin\theta(\cos\theta\cos\varphi\sin 2\psi - \cos\varphi\cos 2\psi)]^2 \\ +0.5\times[f\sin\theta(\cos\theta\sin\varphi\sin 2\psi - \cos\varphi\cos 2\psi)]^2 \end{Bmatrix} + \gamma$
	Parallel	$I = \Lambda \begin{Bmatrix} 2\times[-e\sin\theta\sin\psi(\sin\varphi\cos\psi - \cos\theta\cos\varphi\sin\psi)]^2 \\ +2\times[f\sin\theta\sin\psi(\cos\varphi\cos\psi - \cos\theta\sin\varphi\sin\psi)]^2 \end{Bmatrix} + \gamma$
Model II		$\Re_{Ag} = \begin{vmatrix} a & 0 & 0 \\ 0 & a & 0 \\ 0 & 0 & c \end{vmatrix}$ $\Re_{B_{2g}+B_{3g}} = \begin{vmatrix} 0 & 0 & e \\ 0 & 0 & e \\ e & e & 0 \end{vmatrix}$
A_g	Cross	$I = \Lambda[\sin\psi\cos\psi(a - c\sin^2\theta) - a\cos^2\theta\sin\psi\cos\psi]^2 + \gamma$
	Parallel	$I = \Lambda[c\sin^2\theta\sin^2\psi + a(\cos^2\psi + \cos^2\theta\sin^2\psi)]^2 + \gamma$
$B_{2g} + B_{3g}$	Cross	$I = \Lambda[e^2\sin^2\theta(\cos^{22}\psi + \cos^2\theta\sin^2 2\psi)] + \gamma$
	Parallel	$I = \Lambda[e^2\sin^2\theta\sin^2\psi(\cos^2\psi + \cos^2\theta\sin^2\psi)] + \gamma$

[a] The obtained equations differ depending on the model considered in describing the microstructure of the PE fiber.

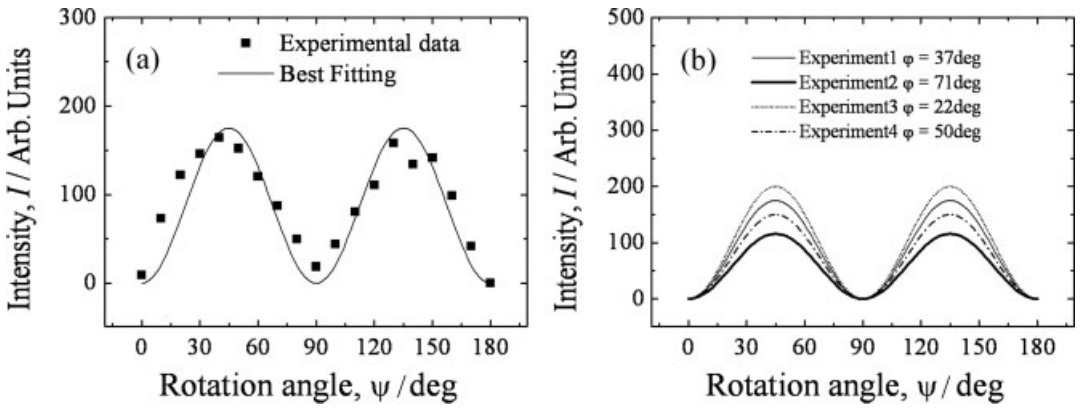

Figure 2. Example of angular dependence of the Raman band intensity at 1293 cm^{-1} retrieved in parallel polarization (a). The least-square fitting curves refer to Model I, while the equations for the $B_{2g} + B_{3g}$ mode in parallel probe configuration were taken as listed in Table 1. In (b), least-square fitting curves of experiments at four different locations along an isolated fiber (monofilament) are compared, and the respective φ angles explicitly reported in inset.

patterns.[28] Note that, in the computational process, we might exclude in first approximation any azimuthal dependence and assume that the orientation distribution function in the fiber is only dependent on the polar angle β (i.e. assuming uniaxial symmetry with respect to the long axis of the fiber). As long as Model I holds validity for the structure of the fiber, one might assume that focusing the laser on different isolated fibers (or at different locations of the same fiber) should lead to a different angular dependence of Raman band intensities, which is characterized by different values of φ. In other words, any different experiment carried out by rotating in-plane the jig supporting the fiber (i.e. rotation by an angle ψ) and keeping the laser focused at exactly the same location should reveal a preferential orientation of the *a* and *b* axis, which should be different from one experiment to another. Note also that, even considering both the available vibrational modes (i.e. A_g and $B_{2g} + B_{3g}$), one cannot retrieve the full set of five (unknown) tensor elements by just collecting two differently polarized Raman intensities at a given angle ψ (and with focusing the probe at a fixed location), because in that case only four independent equations become available (Table 1). However, by collecting the Raman intensity dependences at discrete locations over a given interval of the in-plane rotation angle ψ, a series of independent equations become available. In the computational practice, at a given location in the fiber, a total of nine unknown parameters, namely five Raman tensor elements (i.e. *a*, *b*, *c*, *e*, and *f*), two unknown Euler angles (φ, θ), and two order parameters $\langle P_i(\cos\beta)\rangle$ (with $i = 2,4$), need to be determined (i.e. in addition to two instrumental constants Λ and γ). On the other hand, the constants *A*, λ_2, and λ_4 can be obtained from the additional Eqns (7)–(9). Accordingly, for fully retrieving all the unknown parameters one would need a series of $n \geq 3$ Raman spectra taken at different ψ angles of each location in the in-plane angular interval $0 \leq \psi \leq \pi/2$. A computer routine was then run to obtain least-square fitting curves to experimental plots that, in the present experimental protocol, included $n = 9$ angular values (thus exceeding the

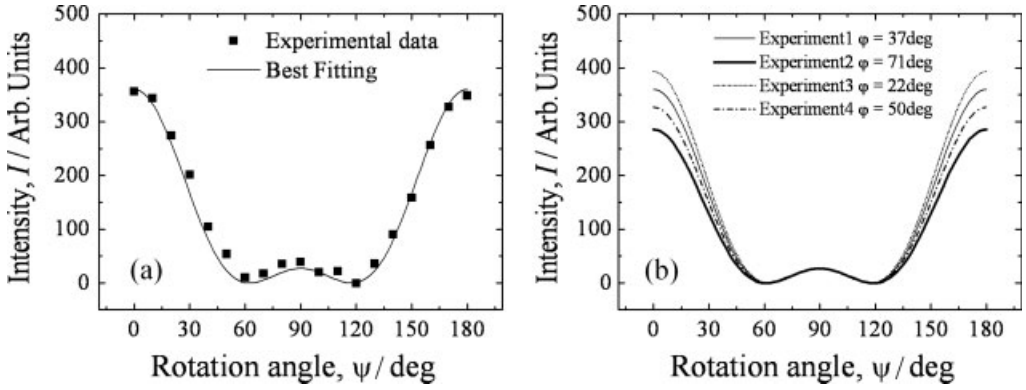

Figure 3. Example of angular dependence of the Raman band intensity at 1130 cm^{-1} collected in parallel polarization (a). The least-square fitting curves refer to Model I, while the equations for the A_g mode in parallel probe configuration were taken as listed in Table 1. In (b), least-square fitting curves are compared for experiments at four different locations along an isolated fiber. Note that the φ angles retrieved in the four different experiments were the same as those calculated by means of the equations concerning the $B_{2g} + B_{3g}$ mode.

minimum number $n = 3$ of needed spectral rotations). It should be noted that the computational routine should locate five tensor elements whose values are independent of probed location, being parameters intrinsic to the crystal structure. On the other hand, the other unknown parameters should be location-dependent. The structure of Raman selection rules pertaining to Model II is also shown in Table 1. The computational routine can be similarly operated to find the unknown parameters (reduced to six in addition to the two instrumental constants, since the model assumes $a = b$ and $e = f$, and any dependence on the φ angle is now lost). Typical angular dependences and their related best fitting curves experimentally retrieved at a randomly selected location on an isolated PE fiber are shown in Figs 2 and 3 for $(B_{2g} + B_{3g})^{||}$ and $A_g^{||}$ modes, respectively. Least-square fitting of the experimental periodic dependences (according to Eqns (3) and (4) and the Raman selection rules given in Table 1 for Model I) led to the values −0.762, −0.944, 0.240, 0.896, and 0.622 for the Raman tensor elements a, b, c, e, and f, respectively. These values satisfied a set of data collected at ten random locations on an isolated fiber (only one set is shown in (a) of each figure for brevity), collected as a function of in-plane rotation angle ψ. The value of the Herman's parameter was found to be always $\langle P_2(\cos\beta)\rangle \geq 0.97$ at any investigated location, thus confirming the extremely high degree of alignment of the PE structure along the long axis of the fiber. Typical values for the remaining parameters were $\langle P_4(\cos\beta)\rangle = 0.92$, $\lambda_2 = \lambda_4 = -10$, and $A = 3.29 \times 10^{-9}$. A striking feature here was that, in the angular dependences collected at different locations, Raman intensities strictly obeyed the predicted periodicities but with different maximum values at $\psi = \pi/4$, $3\pi/4$, and $\psi = 0, \pi$, for the $B_{2g} + B_{3g}$ and A_g modes, respectively. These differences cannot be explained according to the simplified structural Model II. As a matter of fact, fitting of the retrieved experimental data cannot be achieved at any location by means of the same set of five tensor elements unless different values of the φ angle are conceived for different locations (compare best-fitting plots and φ angle values in Figs 2(b) and 3(b)). This finding proves the validity of the domain-like model proposed by Rieckel *et al.*[18] (i.e. Model I) and disproves the isotropic model proposed by Dees and Spruiell[20] (i.e. Model II). Note that a least-square fitting routine on the shown series of experimental data as a function of the in-plane angle ψ can be also obtained for Model II, but only upon normalization of the experimental plots to their respective maxima. This procedure is indeed incorrect and leads to wrong values of the tensor elements (i.e. $a = b$, c, and $e = f$ can be calculated as −0.916, 0.260, and 1.160, respectively). A parametric study of all the angular dependences of the Raman intensity of orthorhombic structures with different sets of Raman tensor elements showed a predominant role of the ratio a/b on the morphology of the parallel-polarized dependence of the $A_g^{||}$ modes on the in-plane rotation angle ψ. In other words, for orthorhombic structures, whose Raman tensor element ratio lies within the interval $0.75 \leq a/b \leq 0.85$ (i.e. including the case of the orthorhombic PE structure for which $a/b \approx 0.8$), the dependence of the Raman selection rules on the angle φ is not negligible.

Conclusion

In conclusion, an in-depth sensitivity study of the Raman selection rules for the orthorhombic structure of a highly aligned PE fiber sample, considering three Euler angles in space as well as the role of orientation distribution functions, allowed us to unfold a set of five Raman tensor elements and, incidentally, to prove the validity of a structural model, as proposed by previous authors, involving the existence of discrete domains in PE fibers with typical dimensions in the order of few micrometers. The knowledge of the set of Raman tensor elements opens the possibility of quantitatively evaluating unknown orientation patterns for PE molecular chains in space (i.e. in the case of PE biomedical grades) by means of polarized Raman spectroscopy.

Supporting information

Supporting information may be found in the online version of this article.

References

[1] J. P. Collier, L. C. Sutula, J. H. Currier, R. E. Wooding, I. R. Williams, K. B. Farber, M. B. Mayor, *Clin. Orthop. Relat. Res.* **1996**, *333*, 76.
[2] D. F. Farrar, A. A. Brain, *Biomaterials* **1997**, *18*, 1677.
[3] S. M. Kurtz, in *The UHMWPE Handbook, Ultra-High-Molecular-Weight-Polyethylene in Total Joint Replacement*, (Ed: S. M. Kurtz). Elsevier Academic Press: New York, **2004**.
[4] P. C. Oparaugo, I. C. Clarke, H. Malchau, P. Herberts, *Acta Orthop.* **2001**, *72*(1), 22.
[5] Y. H. Zhu, K. Y. Chiu, W. M. Tang, *J. Orthop. Surg.* **2001**, *9*(1), 91.

[6] S. P. James S. Blazka, E. W. Merrill, M. Jasty, K. R. Lee, C. R. Bragdon, W. H. Harris, *Biomaterials* **1993**, *14*, 643.
[7] S. M. Kurtz, L. Pruitt, C. W. Jewett, R. P. Crawford, D. J. Crane, A. A. Edidin, *Biomaterials* **1998**, *19*(21), 1989.
[8] R. W. Meyer, L. Pruitt, *Polymer* **2001**, *42*, 5293.
[9] D. J. Crane, L. Pruitt, S. M. Kurtz, C. M. Rimnaca, A. A. Edidin, in *Transactions of the 25th Society for Biomaterials*, vol. 22, **1999**, 515.
[10] S. M. Kurtz, C. M. Rimnac, L. Pruitt, C. M. Jewett, V. Goldberg, A. A. Edidin, *Biomaterials* **2000**, *21*(3), 283.
[11] Ph. Colomban, J. M. Herrera Ramirez, R. Paquin, A. Marcellan, A. Bunsell, *Eng. Fract. Mech.* **2006**, *73*, 2463.
[12] M.-E. Rousseau, T. Lefevre, L. Beaulieu, T. Asakura, M. Pezolet, *Biomacromolecules* **2004**, *5*, 2247.
[13] G. R. Strobl, W. Hagedorn, *J. Polym. Sci. Polym. Phys. Ed.* **1978**, *16*, 1181.
[14] A. E. Zachariades, W. T. Mead, R. S. Porter, *Chem. Rev.* **1980**, *80*, 351.
[15] Z. Ye, S. Zhu, J. F. Britten, *Macromol. Rapid Commun.* **2006**, *27*, 1217.
[16] G. M. Sze, J. E. Spruiell, J. L. White, *J. Appl. Polym. Sci.* **1976**, *20*, 1823.
[17] S. Frisk, R. M. Ikeda, D. B. Chase, J. F. Rabolt, *Appl. Spectrosc.* **2004**, *58*(3), 279.
[18] C. Riekel, A. Cedola, F. Heidelbach, K. Wagner, *Macromolecules* **1030**, *30*, 1033.
[19] G. Pezzotti, T. Kumakura, K. Yamada, T. Tateiwa, L. Puppulin, W. Zhu, K. Yamamoto, *J. Biomed. Opt.* **2007**, *12*, 1.014011.
[20] J. R. Dees, J. E. Spruiell, *J. Appl. Polym. Sci.* **1974**, *18*, 1053.
[21] G. Turrell, in *Practical Raman Spectroscopy* (Eds: D. J. Gardiner, P. R. Graves), Springer: Berlin, **1989**, p 13.
[22] M. S. Amer, J. Maguire, L. Cai, R. Biggers, J. Busbee, S. R. LeClair, *J. Appl. Phys.* **2001**, *89*, 8030.
[23] S. P. S. Porto, R. S. Krishnan, *J. Chem. Phys.* **1967**, *47*, 1009.
[24] R. Loudon, *Adv. Phys.* **1964**, *13*, 423.
[25] M. Pigeon, R. E. Prud'homme, M. Pézolet, *Macromolecules* **1991**, *24*, 5687.
[26] M. J. Citra, D. B. Chase, R. M. Ikeda, K. H. Gardner, *Macromolecules* **1995**, *28*, 4007.
[27] G. Y. Nikolaeva, L. E. Semenova, K. A. Prokhorov, S. A. Gordeyev, *Laser Phys.* **1997**, *7*(2), 403.
[28] R. P´{e}rez, S. Banda, Z. Ounaies, *J. Appl. Phys.* **2008**, *103*, 074302.
[29] E. T. Jaynes, *Phys. Rev.* **1957**, *106*, 620.